Chemosphere 351 (2024) 141225

Contents lists available at ScienceDirect

Chemosphere

journal homepage: www.elsevier.com/locate/chemosphere

The photo- and microbial degradation kinetics and pathways of sulfadoxine in seawater elucidated by liquid chromatography coupled with time-of-flight mass spectrometry

Guowen Tang, Yuling Chen, Shanshan Lin, Xiaolin Li *

State Key Laboratory of Marine Environmental Science, College of Ocean and Earth Sciences, Xiamen University, Xiamen, China

HIGHLIGHTS

- Photo- and microbial degradation processes govern the removal of SDX in seawater.
- An integrated data processing workflow is established for screening high-resolution mass spectra.
- Photo- and microbial degradation pathways of SDX present in marine environment.

GRAPHICAL ABSTRACT

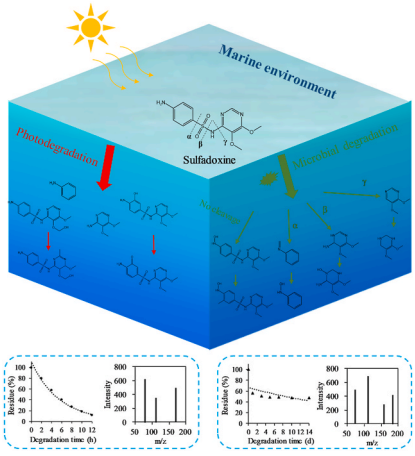

ARTICLE INFO

Handling editor: Keith Maruya

Keywords:
Sulfadoxine
Photodegradation
Microbial degradation
Degradation products
LC-QToF-MS

ABSTRACT

Sulfadoxine (SDX) is a broad-spectrum veterinary antibiotic, which was used alone for the treatment of various infections in the past, and detected ubiquitously in the aqueous environment. However, understanding SDX's photo- and microbial degradation within the environment, especially in marine matrixes, remains limited. This research hones in on SDX's degradation dynamics in seawater. Photodegradation emerges as the dominant process, surpassing microbial degradation in speed and efficiency. Notably, 90% of SDX is photo-degraded within 12 h, while only 52% is removed via microbial degradation over two weeks. Time-of-flight mass spectrometry provides high-resolution molecular mass information on degradation products. The molecular structures of hydrolysis, photo-, and microbial degradation products are deduced from accurate precursor and fragment ion masses, alongside an integrated data processing workflow. Six hydrolysis products arise from the treatment, and photodegradation and microbial degradation yield nine and eighteen products, respectively. Molecular insights from these products inform plausible degradation pathways involving hydrolysis, photodegradation, and microbial degradation. Processes like bond cleavage, methylation, hydroxylation, oxidation, reduction, and

* Corresponding author.
E-mail address: xlli@xmu.edu.cn (X. Li).

https://doi.org/10.1016/j.chemosphere.2024.141225
Received 2 September 2023; Received in revised form 24 December 2023; Accepted 12 January 2024
Available online 17 January 2024

methoxylation are identified and associated with degradation. This study presents a comprehensive workflow for acquiring and processing degradation product data linked to emerging organic pollutants. Moreover, it contributes to our comprehension of the environmental fate of veterinary drugs in marine ecosystems.

1. Introduction

The livestock and aquaculture industries extensively employ veterinary pharmaceuticals for promoting growth and controlling diseases. Veterinary antibiotics constitute over 70% of the total veterinary pharmaceuticals consumed (Sassman and Lee, 2005), and 30–90% of these antibiotics are excreted unmetabolized in animal feces and urine (Sarmah et al., 2006). These veterinary antibiotics can find their way into the aquatic environment through the direct discharge of waste from livestock farms or the accidental release of land fertilizers (Boxall and Long, 2005; Kemper, 2008). Additionally, aquaculture and municipal wastewater are also potential sources of these compounds in aquatic ecosystems (Karthikeyan and Meyer, 2006). Consequently, veterinary antibiotics have been detected in wastewater from livestock farms and municipal treatment plants, ranging from ng/L to μg/L (Campagnolo et al., 2002; Ben et al., 2013; Li et al., 2013), and have been found ubiquitously in riverine and estuarine environments (Xu et al., 2007; Tamtam et al., 2008; Zheng et al., 2011).

The presence of residual veterinary pharmaceuticals and their metabolites in water poses a potential risk to organisms and human health (Witte, 1998). Concerns regarding toxicology have led to an increasing interest in understanding the fate of veterinary pharmaceuticals in natural aqueous environments. Previous studies have demonstrated that these compounds can undergo biotic degradation (Li et al., 2011) as well as abiotic degradation through photodegradation and hydrolysis in aquatic settings (Boxall, 2010). Trovó et al. (2009) researched the photochemical transformation of sulfamethoxazole (SMX) in various water matrices under simulated sunlight. Their study aimed to assess the persistence, toxicity, and degradation pathway of SMX, resulting in the identification of six photo-transformation products during SMX photolysis. Ultraviolet (UV) treatment is commonly employed to remove pharmaceuticals in wastewater at sewage treatment plants (STPs) (Maquille et al., 2010). Kawabata et al. (2013) investigated the photodegradation of nine pharmaceuticals in the aquatic environment using sunlight and different wavelengths of UV irradiation (UV-A, -B, and –C). They concluded that the photodegradation rates of the compounds were influenced by both their chemical structure and the specific wavelength of UV exposure. In another study, Quintana et al. (2005) examined the laboratory degradation of five acidic drugs under aerobic conditions using activated sludge inoculation and analyzed the resulting microbial metabolites using liquid chromatography-mass spectrometry (LC-MS). Preliminary identification of some biodegradation intermediates was achieved through batch tests.

Sulfonamides (SNs) are a prominent group of synthetic bacteriostatic veterinary antibiotics widely utilized in animal husbandry, and their presence in the environment has been frequently detected (Baran et al., 2011). One major chemical form of SNs is sulfadimethoxine (SDMX), whose microbial degradation processes and dynamics in manure-amended soil were investigated by Wang et al. (2006), and a successful application of a kinetic model was observed in fitting the degradation of this specific compound. Another member of the SNs group is sulfadoxine (SDX), a broad-spectrum veterinary antibiotic that was historically employed as a standalone treatment for various infections (Kapoor, 1988). The occurrence of SDX was studied in soil fertilized with animal manures in Eastern China, revealing maximum concentrations reaching 1163 μg/kg (Wei et al., 2016). Limited information exists concerning the environmental fate of SDX, particularly regarding its dynamics and pathways of photo- and microbial degradation, as well as the identification of its metabolites in aquatic environments.

High-resolution mass spectrometry has emerged as a powerful analytical tool for investigating emerging organic pollutants in the environment (Krauss et al., 2010; Shad et al., 2020). One such technique is ultra-high-performance liquid chromatography coupled with quadrupole-time-of-flight mass spectrometry (UPLC-QToF-MS), which can perform quantitative analysis and simultaneous full-scan screening for unknown compounds. Furthermore, it enables the acquisition of accurate mass information for both parent compounds and their metabolites (Castro-Perez et al., 2005; Li and Brownawell, 2009; Mortishire-Smith et al., 2005; Shad et al., 2018; Zhuang et al., 2019). By combining high-resolution mass spectrometry with statistical data processing platforms and chemical searching libraries, a more comprehensive assessment of the sources and fate of emerging organic pollutants in the environment can be achieved (Ni et al., 2010). UPLC-QToF-MS has been successfully employed for identifying photo- and microbial degradation products and proposing pathways of veterinary antibiotics in water and soil (Ibáñez et al., 2004; Manna et al., 2017; Chen et al., 2021). However, a more systematic screening procedure is required to enable accurate characterization of degradation products and offer valuable insights into the transformation pathways of these compounds.

In this study, we aimed to 1) investigate the degradation kinetics of SDX in the aquatic environment, encompassing both photo- and microbial degradation processes, and 2) elucidate the transformation products and pathways of SDX in natural aqueous environments using time-of-flight mass spectrometry. Through our research, we conducted the first comprehensive examination of both photo- and microbial degradation of SDX, thereby enhancing our understanding of the occurrence and fate of antibiotics in marine environments. The findings of this study provide valuable insights into the environmental behavior of SDX and contribute to the broader understanding of antibiotic pollution in aquatic ecosystems.

2. Materials and methods

2.1. Chemicals

The SNs standard of SDX (>96%) was purchased from Shanghai Aladdin Biochemical Technology Co., Ltd. (Shanghai, China). Solvents used in this study, including chromatography grade methanol and acetonitrile, were obtained from ANPEL Laboratory Technologies (Shanghai) Inc. (Shanghai, China). Acetic acid (>99%) and ammonium acetate (>99.99%) were purchased from Sigma-Aldrich Co., LLC (USA and Japan). All glassware used in this study was baked in a muffle furnace for at least 4 h at 450 °C.

2.2. Photodegradation and hydrolysis experiments

The seawater for the experiment was collected in Xiamen Bay, China (24°28′20″N, 118°11′44″E) (Fig. S1) (Tang et al., 2018), and filtered through pre-combustion GF/F filters (0.70 μm pore size, 142 mm diameter, Whatman) to remove suspended particulate matter (SPM). The physical and biochemical parameters of the seawater including temperature, salinity, dissolved organic carbon (DOC), and bacterial abundance, were listed in Table S1. To initiate the photodegradation experiment, a solution of SDX with an initial concentration of 40 μg/L was prepared by adding it to 50 mL of the sterilized seawater in individual quartz test tubes. The initial concentration was about one order of magnitude higher than the maximum concentration detected in the aqueous environment to ensure the identification of degradation

products (Xiao et al., 2023). The experiment was conducted using a solar simulator equipped with a 1000 W xenon lamp (Fig. S2), which emits high-intensity radiation across the full range of sunlight. The quartz test tubes were placed in a thermostatic water bath with a water depth of 1 cm and approximately 1 m away from the lamp source and subjected to irradiation for specific time intervals of 0, 2, 4, 6, 8, 10, and 12 h. The light intensity during the experiment was approximately 1100 lux, which corresponds to the average daytime light intensity in a subtropical region during summer. The thermostatic water bath was set at a temperature of 26 °C to maintain a consistent environment. To study the dynamics of the hydrolysis reaction of SDX, spiked test tubes wrapped in aluminum foil were also irradiated for 12 h and sampled at specific time intervals. Following exposure, the samples were diluted 100 times using a water/methanol mixed solution (9:1, v:v) and stored at 4 °C for subsequent analysis and determination.

2.3. Microbial degradation of SDX in the seawater

Microbial degradation of SDX was investigated in the filtered seawater samples collected from the same site as photodegradation. The physical and biogeochemical parameters of the seawater are listed in Table S1. The sample for bacterial community analyses (1 L) was filtered through 0.2-μm polycarbonate filters (Millipore) under a pressure of <0.03 MPa. Samples for bacterial abundance were fixed with glutaraldehyde at a final concentration of 1% (Vaulot et al., 1989) and frozen in liquid nitrogen prior to storage at −80 °C. Bacterial abundance was measured using a flow cytometer (Becton Dickinson) after staining with SYBR Green I (Marie et al., 1997). Bacterial diversity and communities were monitored by the PCR amplified 16S rRNA genes (Zhang et al., 2014). To determine the functional potential of bacterial community, taxonomically annotated operational taxonomic units (OTUs) were related to metabolic function groups using Functional Annotation of Prokaryotic Taxa (FAPROTAX v.1.1). An output functional table was created with 34 functional groups as shown in Fig. S3. In a pre-cleaned bottle wrapped in aluminum foil to protect from sunlight, 50 ng of SDX was spiked into 100 mL of the filtered seawater. The degradation experiment was conducted in the laboratory at room temperature (25 °C). Time series samples were collected at specific intervals of 0, 1, 3, 5, 7, 10, and 14 days. The sample extraction procedure was modified from the previous report (Li et al., 2013), and generally, the samples were spiked with 100 ng of surrogate standards (SDX-d3) and subjected to solid-phase extraction using Oasis HLB cartridges (500 mg, Waters, Ireland). The analytes were eluted using 10 mL of methanol and 5 mL of a mixed solution of acetonitrile and acetone (1:1, v:v). The eluent was then evaporated to dryness under a gentle nitrogen stream. Finally, 0.9 mL of a water/methanol mixed solution (9:1, v:v) and 0.1 mL of a 100 ppb internal standard (propamocarb-d7) were added to the vial, and the mixture was transferred to an injection vial for instrumental analysis.

2.4. Liquid chromatographic conditions

The chromatographic separation was conducted using a Waters Acquity H-class UPLC system (Waters Corp., Milford, MA, USA) equipped with a BEH C18 2.1 × 50 mm, 1.7 μm column (Waters Corp., Wexford, Ireland) as the stationary phase. The mobile phase consisted of two components: phase A, water with 0.1% acetic acid and 0.1% ammonium acetate, and phase B, a mixture of methanol and acetonitrile in a 1:1 ratio (v:v). A gradient elution method was employed at a flow rate of 0.3 mL/min, with the following program: 0.0–1.0 min, 10% B; 1.0–15.0 min, 90% B; 15.0 min–17.0 min, 90% B; 17.0–17.1 min, 10% B; 17.1 min–19.0 min, 10% B. The volume injected for each sample was 10 μL.

2.5. Mass spectrometry conditions

A Xevo G2-XS Q-ToF mass spectrometer (Waters Corp., Milford, MA, USA) equipped with an electrospray ionization (ESI) interface operating in positive ionization mode was utilized for analysis. The ESI conditions included a capillary voltage of 2.0 kV in ESI^+, with a sample cone voltage of 40 V in some cases. Mass data were acquired over a range of 50–1200 Da with a scan time of 0.5 s in a continuum mode. The source temperature was set to 120 °C, while the desolvation temperature was set to 400 °C. Nitrogen was used as the desolvation gas at a flow rate of 600 L/h, and the cone gas flow rate was set at 50 L/h. The acquisition mode was MS^E, allowing simultaneous acquisition of precursor and fragment ion information. Precursor ions data were collected using a collision energy of 4 eV (low-energy function), while fragment ions data were obtained using a collision energy ramp of 15–40 eV (high-energy function). The precursor and fragment ions were matched based on the same retention time. For calibration, a 0.5 mM sodium formate solution diluted with isopropyl alcohol: water (9:1, v:v) was used at a flow rate of 5 μL/min. Calibration was performed in the mass range of m/z 50 to 1200. During data acquisition, mass-to-charge ratio calibration was achieved using an external reference (Lock-SprayTM) comprising a continuously injected solution of 200 pg/mL leucine-enkephalin (Waters Corp., Milford, MA, USA). The reference ion was generated at m/z 556.2771 in positive mode and at m/z 554.2615 in negative mode, allowing real-time mass correction for maintaining mass accuracy and reproducibility. The Q-ToF resolution was approximately 23000 FWHM (m/z 556.2771).

2.6. Screening and identification of the degradation products

The workflow of data processing for putative degradation products is shown in Fig. S4. Under the optimized UPLC-QToF-MS conditions, an accurate-mass database was established, containing information such as retention time, calculated mass, elemental composition, and isotope details. Commercial software (UPLC-MS^E and MassLynx) were utilized for the collection and rapid screening of mass spectrometry information, respectively. All the MS^E raw data were subsequently transferred to the UNIFI platform provided by Waters for data processing. The UNIFI platform offers an integrated approach for data acquisition, data mining, library search, and metabolite prediction, enabling the efficient processing of large data sets and extraction of meaningful results from complex data sets (Kang et al., 2017; Mi et al., 2019; Chen et al., 2021). By leveraging the integrated data processing informatics platform, UNIFI, the structures of degradation products and proposed pathways can be inferred (Ibáñez et al., 2004; Ni et al., 2010; Manna et al., 2017).

In the UNIFI platform, the data was extracted in 3D peaks using two functions: one for the low-energy (LE) function with an intensity threshold of 100, and one for the high-energy (HE) function with an intensity threshold of 1000. In positive ionization mode, the adduct ions, e.g. $+H$, $+Na$, and $+NH_4$, were selected. For the identification of degradation products, several parameters were employed based on previous studies (Thurman et al., 2005, 2013; Little et al., 2011; Sánchez-Hernández et al., 2016; Bauer et al., 2018). To ensure accuracy, suspicious mass peaks were filtered before determining the elemental composition using the software. These parameters include a mass accuracy tolerance of ±5 mDa for the precursor ion. The retention time error for all samples was kept below 0.3 min. Additionally, the presence of one or more characteristic fragment ions with a mass error of less than 10 mDa was required for identification purposes.

After the above screening, manual screening was still required in two steps: (1) the Total Ions Chromatograph (TIC) and 3D LC-MS plot were compared with blank samples and 0-h samples, and the characteristic peaks that appeared in the experimental samples were selected. To find the corresponding substance in the component, the substance was very likely to be a theoretically predictable product, and its possible structure should be inferred by combining the mass of the parent ion and fragment ions. Due to the limited resolution scale of the TIC and 3D LC-MS plot, the method can only identify related products when the response value of products was high. Most of the products did not show obvious

characteristic peaks in the TIC and 3D LC-MS plots, and further screening was needed to determine the information on other products. (2) For products without obvious characteristic peaks in TIC and 3D LC-MS plot, Mass Defect Filter (MDF), Neutral Loss Filter (NLF), Element Composition Analysis (ECA), ChemSpider online database Search (CS) combined with the binary comparison with blank samples, 0-h samples, and trend chart comparison, to find products information with a good matching degree. Finally, the Mass Fragment™ function with chromatographic interpretation function and Fragment Match (FM) were combined to determine or characterize the structure of the detected products. Using this feature, we could quickly verify that the fragmented path was reasonable and thus finalize all the product information.

3. Results and discussion

3.1. The dynamics of the photo- and microbial degradation of SDX

As illustrated in Fig. 1, the photodegradation of SDX exhibited pronounced progress within 12 h, leading to the degradation of approximately 90% of the initially spiked compounds. Concurrently, the hydrolysis process resulted in the breakdown of around 20% of the SDX (Fig. 1a). To quantitatively assess the degradation kinetics of SDX, the first-order reaction model, as previously described by Li et al. (2011), was employed. The degradation process of SDX is represented by the following equations:

$$-\ln(C_t / C_0) = k \cdot t \quad (1)$$

$$T_{1/2} = \ln 2 / k = 0.693 / k \quad (2)$$

Where equation (1) represents the first-order kinetic equation, and C_t and C_0 are the concentrations at a certain degradation time (t) and the initial time (t_0), respectively, k is the degradation rate constant. Equation (2) represents the half-life of SDX ($T_{1/2}$) estimated by the degradation rate constant. Both the hydrolysis and photodegradation processes of SDX exhibit first-order degradation kinetics, characterized by rate constants (k) of 0.020 and 0.179, respectively. Correspondingly, the $T_{1/2}$ is calculated to be 35.0 h for hydrolysis and 3.9 h for photodegradation. Zessel et al. (2014) investigated the photodegradation reaction of two other sulfonamide veterinary antibiotics, sulfanilamide (SA) and sulfathiazole (STZ), under sunlight conditions. The resulting k values for SA and STZ were 0.008 and 0.010, respectively (as indicated in Table 1). Notably, when subjected to photodegradation treatment using UVB plus UVA, both SA and STZ exhibited relatively higher k values. It was suggested that UVB was a predominant factor in their photodegradation process. This study aligns with earlier research indicating that photochemical degradation plays a pivotal role in determining the environmental fate of sulfonamide antibiotics (SNs). A key characteristic of most SNs is their possession of aromatic rings, heteroatoms, and other functional groups capable of absorbing solar radiation or reacting with photogenerated intermediates present in natural water. These intermediates include reactive oxygen species and light-excited natural organic matter (Boreen et al., 2003). Such features contribute to the susceptibility of SNs to photochemical degradation and underscore the importance of understanding the underlying mechanisms of their fate in environmental matrices.

Microbial incubation of SDX within the seawater initiated a degradation process, resulting in approximately 44% degradation on the initial day, gradually advancing to about 52% over two weeks (as depicted in Fig. 1b). The microbial-driven degradation observed in this study adhered to a first-order reaction model, with the initial labile dissolved organic carbon (DOC), including the spiked SDX, sustaining microbial activity within the treatment. Building upon our previous research (Li et al., 2021), we noted a peak in bacterial abundances within the initial 3 days, followed by a gradual decrease until the experiment's conclusion on the 14th day. A similar trend was observed for

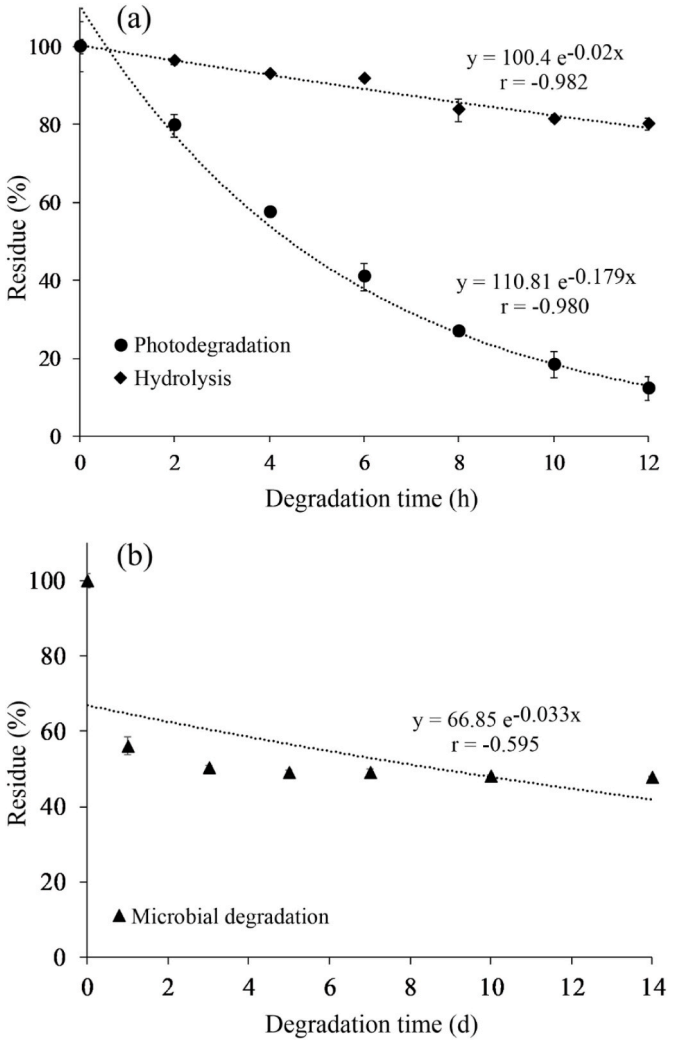

Fig. 1. The hydrolysis and photodegradation (a) and microbial degradation (b) dynamics of SDX in seawater.

Table 1
Degradation rate constant and half-life of different veterinary antibiotics.

Compound	Matrix	Degradation treatment	k	$T_{1/2}$	References
SDX	Seawater	Hydrolysis	0.020	35.0 h	This study
	Seawater	Photodegradation	0.179	3.9 h	
	Non-sterile seawater	Microbial degradation	0.033	20.8 d	
SMX	Non-sterile aquaculture water	Microbial degradation	0.033	21.3 d	Lai et al. (2011)
	Sterile aquaculture water	Microbial degradation	0.011	62.9 d	
SMX	Non-sterile river water	Microbial degradation	0.031	22.3 d	Xu et al. (2011)
	Sterile river water	Microbial degradation	0.006	115.5 d	
SA	Phosphate buffered saline	UVA/UVB exposure	0.268	2.6 h	Zessel et al. (2014)
		Sunlight exposure	0.008	86.6 h	
STZ	Phosphate buffered saline	UVA/UVB exposure	0.271	2.6 h	Zessel et al. (2014)
		Sunlight exposure	0.010	69.3 h	

DOC degradation in the same treatment, characterized by a rapid decline in the initial days and subsequent stability throughout the remaining incubation period. The observed limitation in microbial activity in the experiment may be attributed to the decreasing supply of labile DOC in the closed system. As a result, the degradation of SDX reached a plateau towards the end of the experiment, influenced by the impact of the limited energy supplied by labile organic materials. The functional groups identified from the taxonomic units of the bacterial

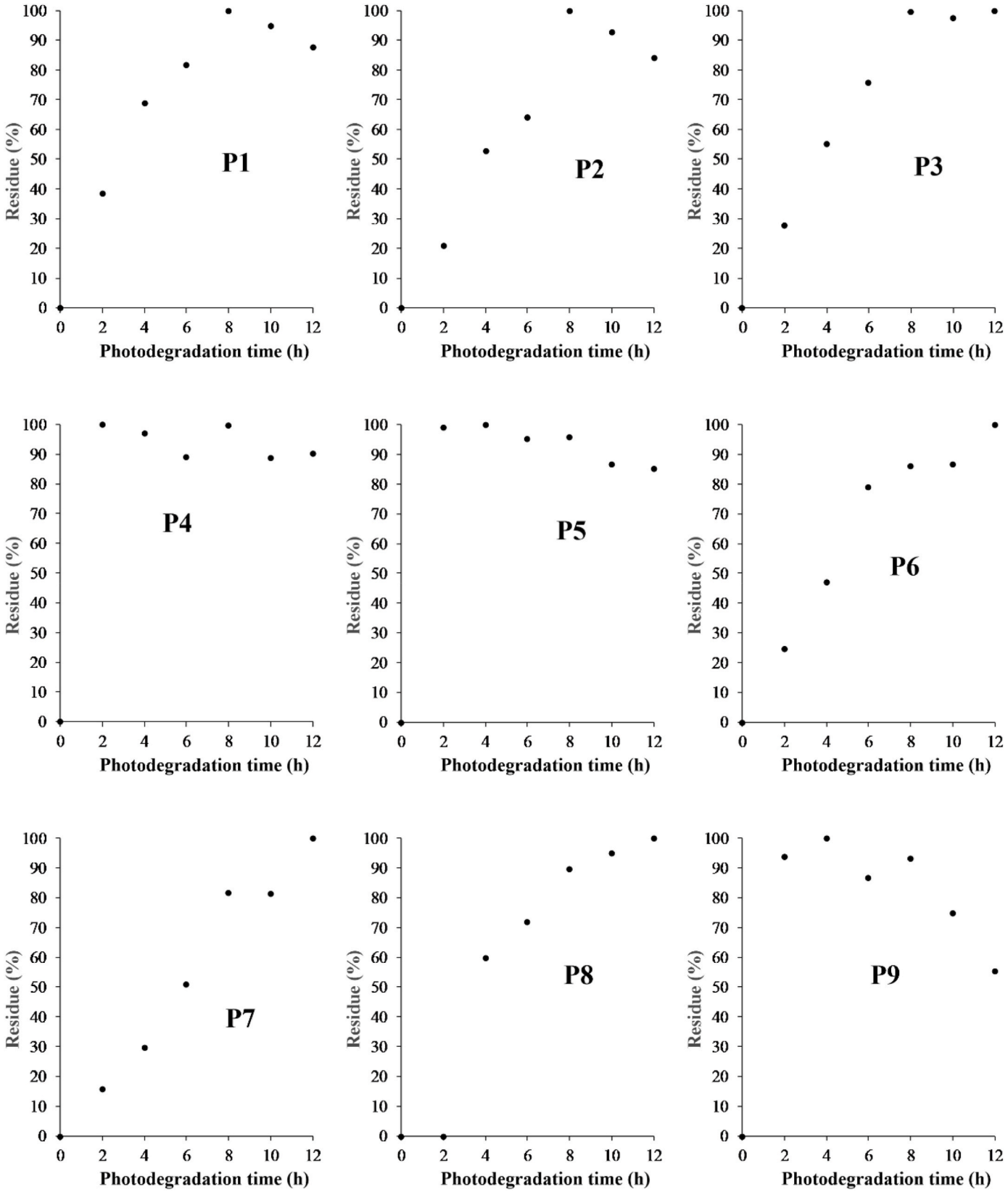

Fig. 2. Variations of the proposed products during photodegradation treatment.

community in the seawater provide additional support for the metabolic transformation of organic materials in the treatment (Fig. S3).

This microbial-driven degradation followed a first-order reaction pattern, with calculated values k and $T_{1/2}$ values of 0.033 and 20.8 d, respectively. In a parallel study, Lai et al. (2011) disclosed microbial degradation rate constants for sulfamethoxazole (SMX) within both non-sterile and sterile aquaculture water, measuring 0.033 and 0.011, respectively. Similar investigations conducted in river water yielded comparable values of 0.041 and 0.006, respectively (Xu et al., 2011). Remarkably, these values closely align with the result observed in this study (refer to Table 1). Their findings confirmed the pivotal role of microbial activities in the degradation of SNs, particularly emphasized through comparisons between sterile and non-sterile treatments. Generally, microbial degradation rates were discernibly slower in comparison to the rates observed for hydrolysis and photodegradation. This contrast in degradation rates underscores the distinct contributions of different degradation pathways and highlights the significance of microbial communities in shaping the fate of SNs in marine aquatic environments.

3.2. Identification of photodegradation and hydrolysis products and their pathways

Detailed in Section 2.6, the data processing workflow facilitated the screening and identification of photodegradation and hydrolysis products of SDX. Visual representation of SDX's molecular structure and potential bond cleavage positions can be found in Fig. S5, while Table S2 compiles all the identified products. Notably, the initial three photodegradation products (P1, P2, and P3) were successfully identified through both the Total Ion Chromatogram (TIC), as illustrated in Fig. S6, and the three-dimensional LC-MS plot, depicted in Fig. S7. These identifications were based on a comparative analysis against the treatment at time 0 h. Both P1 and P2 exhibited a retention time of 1.83 min, whereas P3 displayed a retention time of 2.33 min. Their response levels exhibited a gradual increase with extended irradiation time, as showcased in Fig. 2.

As shown in Fig. S8, The *m/z* of P1 is 360.1335 identified as $[M + NH_4]^+$ ion ($C_{13}H_{18}N_4O_5S$). Fragment ions of P1 at *m/z* 156.01183 and 92.05041 mirror the aniline structure inherent in the precursor (Fig. S5). Additionally, fragment ions observed at *m/z* 147.07698 and 302.08092 suggested that a methyl group's attachment to the C atom links the two N atoms within SDX's pyrimidine ring. As a result of hydroxyl free radicals formed in water under sunlight, organic compounds undergo facile oxidation by these radicals (Hirahara et al., 2003). Based on the mass number derived from secondary mass spectrometry, it is determined that the hydroxyl group is situated on the methoxy group. And hydrogenation and hydroxylation reactions contribute to the generation of P1. The *m/z* of P2 is 324.0617, denoting the $[M + H]^+$ ion ($C_{13}H_{13}N_3O_5S$). Analyzing fragment ions, it becomes evident that cleavage of the amino bond transpires, accompanied by the addition of a methyl group onto the C atom that bridges the two N atoms within the pyrimidine ring. Subsequent hydroxylation and oxidation reactions culminate in the formation of P2, as exemplified in Fig. S9. The *m/z* of P3 is 156.0776 identified as $[M + H]^+$ ion ($C_6H_9N_3O_2$) (Fig. S10). Based on the fragment ions, the β bond of SDX was cleaved leading to the creation of 4-amino-5, 6-dimethoxy-pyrimidine (P3), and 4-aminobenzene-1-sulfonic acid. Notably, 4-aminobenzene-1-sulfonic acid is not detectable in our samples when matching the authentic standard. This absence could be attributed to the potential loss of sulfate ions, resulting in the formation of aniline, marked as P4 (C_6H_7N, *m/z* of $[M + NH_4]^+$ ion is 111.0926). P4 emerges in all our degradation samples with a retention time equal to 0.65 min (Fig. 2 and Fig. S11). A similar transformation mechanism was reported in previous studies (Wang et al., 2010; Xin et al., 2020). The elemental composition of P4 is determined via elemental composition analysis with i-FIT confidence of 100% and a mass error of 0.895 mDa.

Distinctive peaks of certain products could not be discerned solely through binary comparisons, and MDF, NLF, ECA, and CS steps were applied to identify the products, as elaborated upon in the previous section. Through these analytical methodologies, an addition of six more degradation products (P4–P9) emerged, which were not visually detected in the TIC diagram (Table S2 and Fig. 2). For instance, the *m/z* of P5 stands at 327.0775, identified as $[M + H]^+$ ion ($C_{12}H_{14}N_4O_5S$) and its retention time is at 12.45 min. Upon analysis of the fragment ion at *m/z* 125.01710, it suggests that hydroxylation occurs within the aniline ring rather than the pyrimidine ring (Fig. S12). The *m/z* of P6 is detected at 325.0598, identified as $[M + H]^+$ ion ($C_{12}H_{12}N_4O_5S$). Fragment ions of P6 were observed at *m/z* 141.07102 and *m/z* 156.99401 pointing toward an oxidation event concerning the hydroxyl group within P5 (Fig. S13). This deduction is proved by the decrement in P5's response throughout photodegradation. The emergence of P7 at *m/z* 246.0875 ($[M + NH_4]^+$ ion, $C_9H_{12}N_2O_3S$) at a retention time of 4.85 min is identified based on the only fragment ion at *m/z* 213.0540. The formation of P7 likely involves the cleavage of bonds within SDX (Fig. S14). P8, characterized by *m/z* 327.0753 and observed as $[M + H]^+$ ion ($C_{12}H_{14}N_4O_5S$), emerged at 1.18 min. Based on the fragment ions, P8 could be formed through the hydroxylation of the SDX's methoxy group (Fig. S15). Lastly, P9, characterized by *m/z* 314.1280 and observed as $[M + NH_4]^+$ ion ($C_{12}H_{16}N_4O_3S$) emerged at 0.75 min. The fragment ions of P9 obtained at *m/z* 156.01157, *m/z* 126.06655 and *m/z* 141.09041 suggest a hydrogenation reaction at the N–C–N bond of the pyrimidine ring, concurrently leading to the cleavage of the methoxy bond (Fig. S16). In Fig. 3, the chromatograms encompassing all photodegradation products are shown, while Fig. 4 includes the proposed photodegradation pathway of SDX in water. These intricate photodegradation pathways encompass bond cleavage, reduction, oxidation, methylation, and hydroxylation reactions, collectively contributing to SDX's transformation.

Hydrolysis product H1 was successfully identified through analysis of both the TIC and 3D LC-MS plots that emerged at 1.17 min in the hydrolysis treatments (Fig. S17 and Fig. S18). H1 presents with an *m/z* of 327.0753, observed as $[M + H]^+$ ions ($C_{12}H_{14}N_4O_5S$). Analysis of fragment ions reveals that H1 shares the same molecular structure as P8. An interesting observation is that the response of H1 surpasses that of P8 after 12 h, potentially indicating that P8 could undergo further degradation and/or transformation into P1 during photodegradation. Through a systematic statistical screening procedure, an additional five hydrolysis products (H2–H6) are identified (Table S2). For instance, H2, characterized by an *m/z* 325.0967, observed as $[M + H]^+$ ions ($C_{13}H_{16}N_4O_4S$), emerges at 6.69 min. Fragment ions of H2 suggest N-methylation within the aniline group, with the nitrogen atom in aniline known for its high reactivity (as evidenced by Boreen et al., 2004) (Fig. S19). H3 with an *m/z* of 236.0342 was observed as $[M + H]^+$ ions

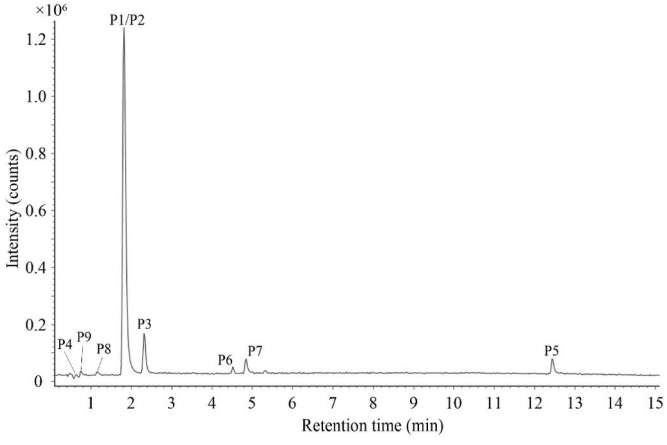

Fig. 3. Chromatogram of the proposed photodegradation products.

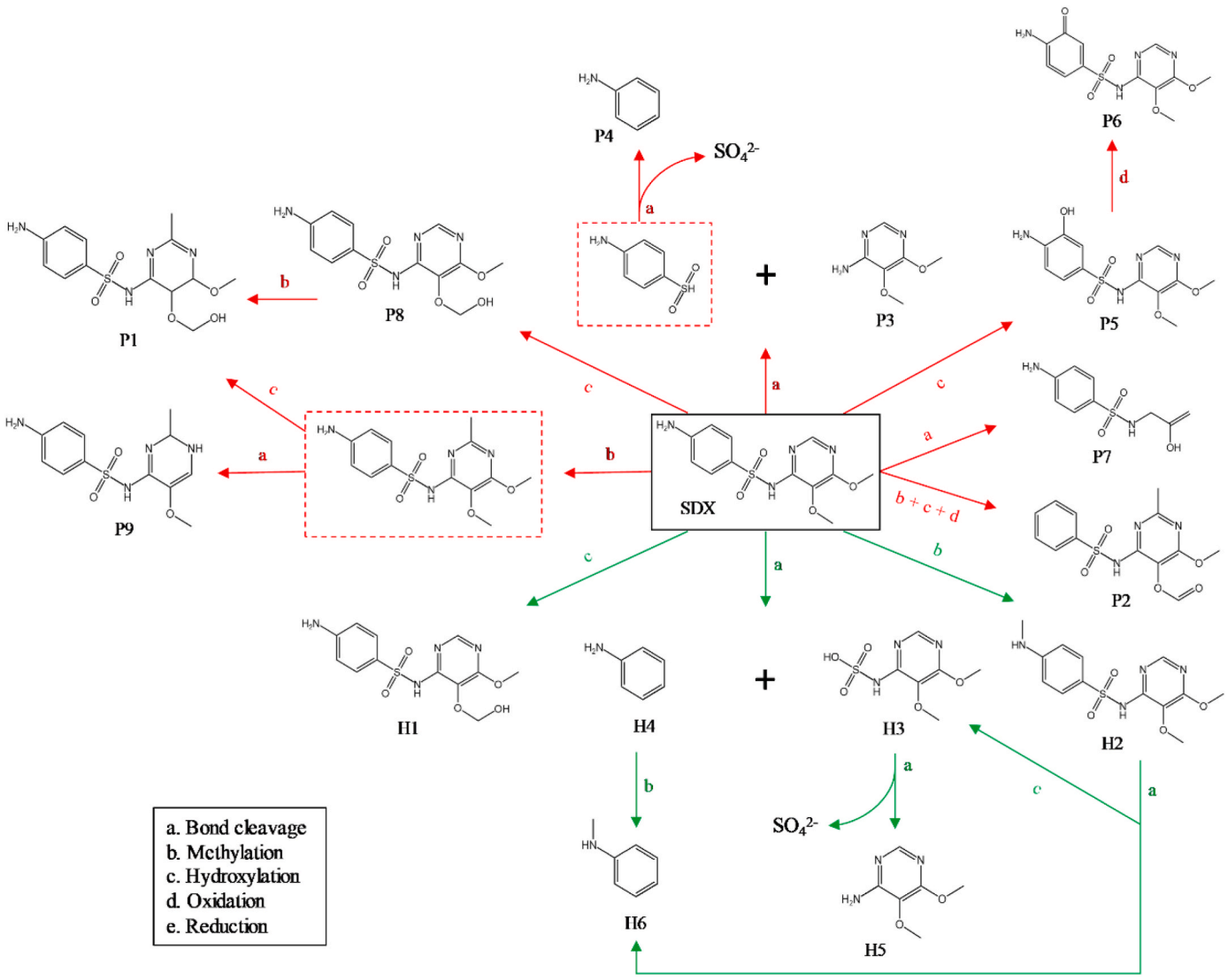

Fig. 4. Proposed pathways of SDX's photodegradation and hydrolysis reactions (The red line stands for the photodegradation pathway and the green line stands for the hydrolysis pathway. The dotted frame includes the proposed intermediate degradation products). (For interpretation of the references to colour in this figure legend, the reader is referred to the Web version of this article.)

($C_6H_9N_3O_5S$) and H4 with an *m/z* of 111.0923 observed as $[M + NH_4]^+$ ions ($C_6H_7N_3$) are proposed to result from α bond cleavage of SDX depending on the fragment analysis (Fig. S20). It is noteworthy that H4 and P4 share identical molecular structures. H5, characterized by an *m/z* 156.0772, observed as $[M + H]^+$ ions ($C_6H_9N_3O_2$) emerging at 0.78 min shares the same structure as P3. Finally, H6, presenting with an *m/z* 125.1082, observed as $[M + NH_4]^+$ ions (C_7H_9N) at 3.03 min, is associated with methylation of the amino group within H5, as deduced from its elemental composition analysis (Fig. S21). Fig. 4 presents the proposed hydrolysis pathways of SDX, highlighting α bond cleavage, methylation, and hydroxylation as the key hydrolysis reactions contributing to its transformation.

3.3. Identification of microbial degradation products and pathways

Based on the same screening and identification procedure described above, an exhaustive roster of 18 microbial degradation products (M1-M18) has been compiled from the microbial degradation treatment. Detailed molecular information of the degradation products is listed in Table S2. For instance, M1 characterized at *m/z* 327.0779, observed as $[M + H]^+$ ($C_{12}H_{14}N_4O_5S$), emerges at 12.58 min. Fragment ions observed at *m/z* 117.0703, 123.0435, and 147.0807 (Fig. S25) indicate the occurrence of hydroxylation on the amino group, contributing to the formation of M1. M2 characterized at *m/z* 341.0933, observed as $[M + H]^+$ ($C_{13}H_{16}N_4O_5S$), presents at 13.28 min. The fragment ions of M2 observed at *m/z* 94.0652, 108.0434, and 122.0608 suggest a tandem hydroxylation and methylation process within the aniline group (Fig. S26). This concurs with prior research indicating that re-entry groups predominantly occupy the ortho (o-) and para (p-) positions (Morrison Thornton, 1983). M3 characterized at *m/z* 314.0890 ($C_{11}H_{12}N_4O_4S$), observed as $[M + NH_4]^+$ ion, elutes at 0.75 min. And M3 originates from the cleavage of a methyl group (-CH_3) from SDX, as illustrated in Fig. S27. M4, emerging at 0.72 min, presents a $[M + NH_4]^+$ ion at *m/z* 111.0922 (C_6H_7N). Notably, M4 aligns with the molecular structure of both P4 and H4, given their identical molecular mass and retention times (Fig. S28). M5 is eluted at 0.72 min and $[M + NH_4]^+$ ion is observed at *m/z* 127.0868 (C_6H_7NO). This implies that M5 is a result of hydroxylation within the aniline group (Fig. S29). M6 is eluted at 0.67 min and $[M + H]^+$ ion is observed at *m/z* 154.1230 ($C_9H_{15}NO$). Fragment ions of M6 are obtained at *m/z* 94.06561 and 148.07454, indicating the occurrence of hydrogenation (+2H) and methylation (+CH_2) occurred on the benzene ring (Fig. S30). M7 is eluted at 11.19

min and $[M + NH_4]^+$ ion is observed at *m/z* 203.1432 ($C_9H_{15}NO_3$). And M7 forms through hydroxylation on the most active ortho- (o-) methyl groups of M6 (Fig. S31). M8 is eluted at 0.81 min and $[M + Na]^+$ is observed at *m/z* 130.0652 (C_7H_9N). It can be deduced that N-Methylaniline (M8) originates from methylation (+CH2) on the aniline group of M4 (Fig. S32). M9 is eluted at 0.70 min and $[M + NH_4]^+$ ion is observed at *m/z* 123.0922 (C_7H_7N). While no specific fragment ion is identified for M9, its formula is ascertained through elemental composition analysis with i-FIT confidence of 100% (shown in Fig. S33). M9 can be identified as N-Methylenebenzenamine, generated through the

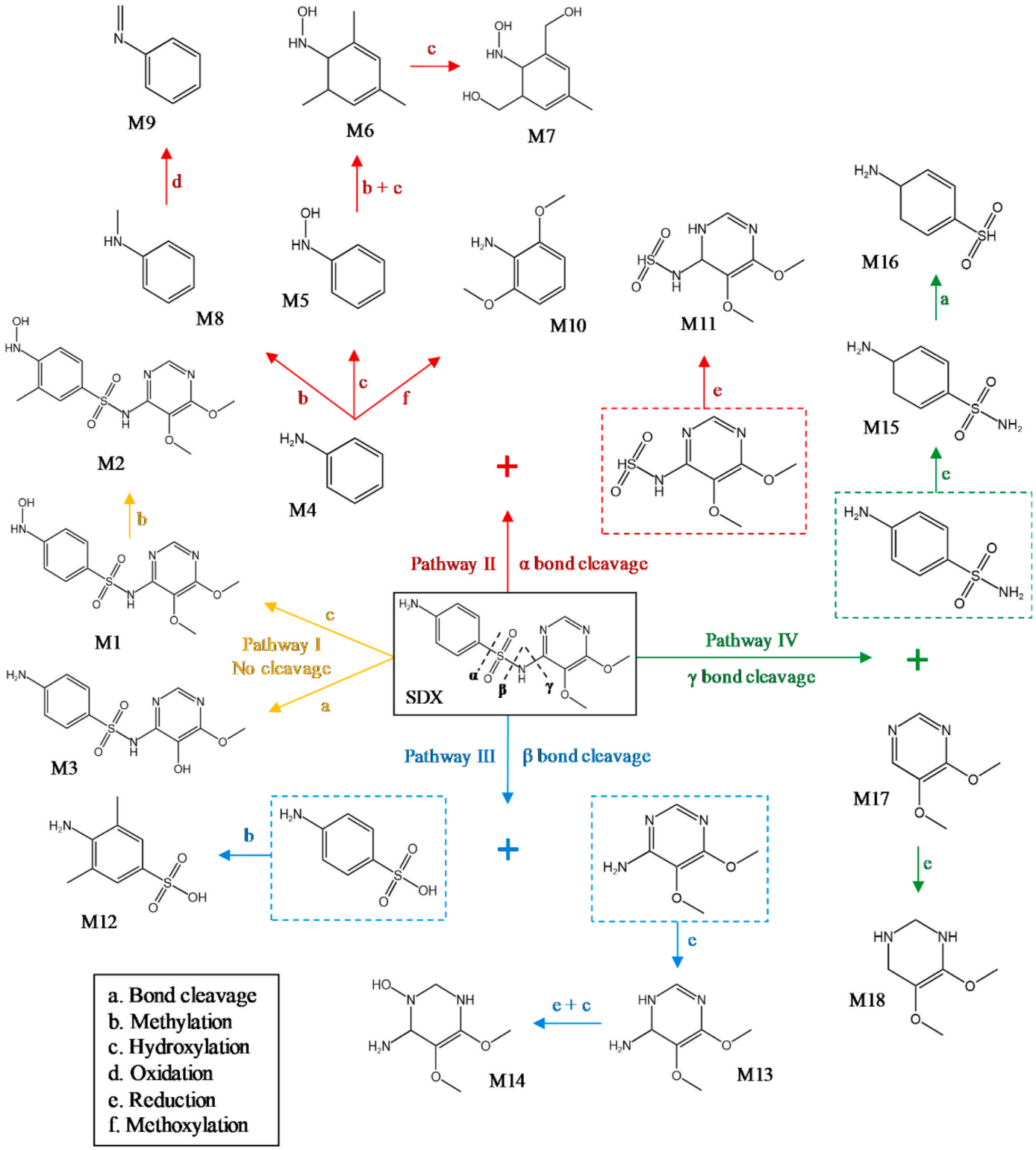

Fig. 5. Proposed pathways of SDX's microbial degradation. (The yellow line represents pathway I with no bond cleavage; the red line represents pathway II with α bond cleavage; the blue line represents pathway III with β bond cleavage; the green line represents pathway IV with γ bond cleavage. The dotted frame includes the proposed intermediate degradation products). (For interpretation of the references to colour in this figure legend, the reader is referred to the Web version of this article.)

oxidation (-2H) of M8. M10 is eluted at 0.72 min and $[M + NH_4]^+$ ion is observed at *m/z* 171.1134 ($C_8H_{11}NO_2$). A fragment ion of M10 is observed at *m/z* 136.07567 suggesting the incorporation of a methoxy group (-OCH_3) from M4 (Fig. S34). M11 is eluted at 0.63 min and $[M + NH_4]^+$ ions are observed at *m/z* 239.0797 ($C_6H_9N_3O_5S$). M11 could be created through α bond cleavage of SDX (Fig. S5), and fragment ions are observed at *m/z* 127.07286 and 129.05094, indicating the presence of pyrimidine rings that have undergone reduction reactions (Fig. S35). Microorganism-mediated processes often induce the reduction of double bonds within pyrimidine rings, transitioning them into single bonds (Singh, 2012). M12 is eluted at 0.54 min and $[M + H]^+$ ion is observed at *m/z* 202.0567 ($C_8H_{11}NO_3S$). M12 originates from the methylation reaction of sulfanilic acid derived from the β bond cleavage of SDX (Fig. S36 and Fig. S37). M13 is eluted at 1.03 min and $[M + NH_4]^+$ is observed at *m/z* 175.1230 ($C_6H_{11}N_3O_2$), likely resulting from the reduction of 4-Amino-5,6-dimethoxypyrimidine (P3), as implied by the fragment ion at *m/z* 125.10872 (Fig. S38). The *m/z* of M14 is 193.1335 ($C_6H_{13}N_3O_3$) with observed $[M + NH_4]^+$ ion and elutes at 5.24 min. M14 probably forms through the hydroxylation of M13 (Fig. S39). M15 is eluted at 4.79 min and $[M + NH_4]^+$ ion is observed at *m/z* 192.0768 ($C_6H_{10}N_2O_2S$), likely resulting from the reduction of SA derived from the γ bond cleavage of SDX (Fig. S40 and Fig. S41). M16 is eluted at 3.18 min and $[M + NH_4]^+$ ion is observed at *m/z* 177.0664 ($C_6H_9NO_2S$), forms through the loss of the amino group from M15, supported by the fragment ion at *m/z* 94.06594 (Fig. S42). M17 is eluted at 9.02 min and $[M + H]^+$ ion is observed at *m/z* 141.0701 ($C_6H_8N_2O_2$), corresponding to 4, 5-dimethoxy pyrimidine, confirmed by the fragment ion at *m/z* 126.0464 (Fig. S43). M18 is eluted at 8.43 min and $[M + H]^+$ ion is observed at *m/z* 145.1018 ($C_6H_{12}N_2O_2$), forming through the reduction of M17 (Fig. S44).

The temporal profiles and chromatograms of the comprehensive set of 18 microbial degradation products are presented in Figs. S23–24 and Fig. S45, respectively. The elucidated microbial degradation pathways of SDX in the marine environment are portrayed in Fig. 5, offering a comprehensive overview of the intricate mechanisms. This study identifies four primary categories of microbial degradation mechanisms. Pathway I: This mechanism involves no bond cleavage, indicating that SDX molecules remain largely intact; Pathway II, III, and IV: α, β, and γ bond cleavage leads to the formation of specific degradation products. These pathways are characterized by a diverse array of reactions, including reduction, oxidation, methylation, hydroxylation, and methoxylation, which collectively contribute to the multifaceted transformation of SDX during microbial degradation.

4. Conclusions

The present study delved into the intricate dynamics of hydrolysis, photodegradation, and microbial degradation of SDX in seawater. For all three degradation mechanisms, the application of a first-order reaction model proved effective in representing their kinetics. Notably, the photodegradation of SDX is proved to be a faster and higher degree of completion in contrast to microbial degradation. To screen and characterize the comprehensive degradation products of SDX, the employment of UPLC-QToF-MS proved pivotal. Through this analytical technique, high-resolution mass spectrometry data were collected, providing an in-depth understanding of the intricate transformation processes. UPLC-MS^E and MassLynx were successfully applied in collecting and scrutinizing the mass spectrometry data of the degradation products. The structural details of these products were inferred based on the precise mass of precursor ions and fragment ions. The degradation pathways are proposed to benefit from the acquired molecular information of the degradation products. By shedding light on the intricate processes that govern the degradation of SDX, this study enriches our comprehension of the environmental behavior and fate of veterinary drugs in marine ecosystems.

CRediT authorship contribution statement

Guowen Tang: Data curation, Writing - original draft. **Yuling Chen:** Data curation. **Shanshan Lin:** Conceptualization, Data curation, Methodology. **Xiaolin Li:** Conceptualization, Data curation, Funding acquisition, Methodology, Project administration, Resources, Writing - original draft, Writing - review & editing.

Declaration of competing interest

The authors declare that they have no known competing financial interests or personal relationships that could have appeared to influence the work reported in this paper.

Data availability

Data will be made available on request.

Acknowledgments

This research was funded by the National Natural Science Foundation of China through grants #42276034. We sincerely thank Dr. Guang Gao and Dr. Kunshan Gao at Xiamen University who provided photo treatment device, and Dr. Tinglin Yang at COMET of Xiamen University for the help on instrumental analysis.

Appendix A. Supplementary data

Supplementary data to this article can be found online at https://doi.org/10.1016/j.chemosphere.2024.141225.

References

Baran, W., Adamek, E., Ziemiańska, J., Sobczak, A., 2011. Effects of the presence of sulfonamides in the environment and their influence on human health. J. Hazard Mater. 196, 1–15.
Bauer, A., Luetjohann, J., Hanschen, F.S., Schreiner, M., Kuballa, J., Jantzen, E., Rohn, S., 2018. Identification and characterization of pesticide metabolites in Brassica species by liquid chromatography travelling wave ion mobility quadrupole time-of-flight mass spectrometry (UPLC-TWIMS-QTOF-MS). Food Chem. 244, 292–303.
Ben, W., Pan, X., Qiang, Z., 2013. Occurrence and partition of antibiotics in the liquid and solid phases of swine wastewater from concentrated animal feeding operations in Shandong Province, China. Environ. Sci.: Process. Impacts 15, 870–875.
Boreen, A.L., Arnold, W.A., McNeill, K., 2003. Photodegradation of pharmaceuticals in the aquatic environment: a review. Aquat. Sci. 65, 320–341.
Boreen, A.L., Arnold, W.A., McNeill, K., 2004. Photochemical fate of sulfa drugs in the aquatic environment: sulfa drugs containing five-membered heterocyclic groups. Environ. Sci. Technol. 38, 3933–3940.
Boxall, A., Long, C., 2005. Veterinary medicines and the environment. Environ. Toxicol. Chem. 24, 759.
Boxall, A.B., 2010. Veterinary medicines and the environment. Comparative and veterinary pharmacology 291–314.
Campagnolo, E.R., Johnson, K.R., Karpati, A., Rubin, C.S., Kolpin, D.W., Meyer, M.T., Esteban, J.E., Currier, R.W., Smith, K., Thu, K.M., 2002. Antimicrobial residues in animal waste and water resources proximal to large-scale swine and poultry feeding operations. Sci. Total Environ. 299, 89–95.
Castro-Perez, J., Plumb, R., Granger, J.H., Beattie, I., Joncour, K., Wright, A., 2005. Increasing throughput and information content for in vitro drug metabolism experiments using ultra-performance liquid chromatography coupled to a quadrupole time-of-flight mass spectrometer. Rapid Commun. Mass Spectrom.: An International Journal Devoted to the Rapid Dissemination of Up-to-the-Minute Research in Mass Spectrometry 19, 843–848.
Chen, K., Liu, X., Wu, X., Xu, J., Dong, F., Zheng, Y., 2021. The degradation dynamics and rapid detection of thiacloprid and its degradation products in water and soil by UHPLC-QTOF-MS. Chemosphere 263, 127960.
Hirahara, Y., Ueno, H., Nakamuro, K., 2003. Aqueous photodegradation of fenthion by ultraviolet B irradiation: contribution of singlet oxygen in photodegradation and photochemical hydrolysis. Water Res. 37, 468–476.
Ibáñez, M., Sancho, J.V., Pozo, Ó.J., Hernández, F., 2004. Use of quadrupole time-of-flight mass spectrometry in environmental analysis: elucidation of transformation products of triazine herbicides in water after UV exposure. Anal. Chem. 76, 1328–1335.
Kang, L.-p., Huang, Y.-y., Zhan, Z.-l., Liu, D.-h., Peng, H.-s., Nan, T.-g., Zhang, Y., Hao, Q.-x., Tang, J.-f., Zhu, S.-d., 2017. Structural characterization and discrimination of the Paris polyphylla var. yunnanensis and Paris vietnamensis based on metabolite profiling analysis. J. Pharmaceut. Biomed. Anal. 142, 252–261.

Kapoor, V.K., 1988. Sulfadoxine. Analytical Profiles of Drug Substances. Elsevier, pp. 571–605.
Karthikeyan, K., Meyer, M.T., 2006. Occurrence of antibiotics in wastewater treatment facilities in Wisconsin, USA. Sci. Total Environ. 361, 196–207.
Kawabata, K., Sugihara, K., Sanoh, S., Kitamura, S., Ohta, S., 2013. Photodegradation of pharmaceuticals in the aquatic environment by sunlight and UV-A,-B and-C irradiation. J. Toxicol. Sci. 38, 215–223.
Kemper, N., 2008. Veterinary antibiotics in the aquatic and terrestrial environment. Ecol. Indicat. 8, 1–13.
Krauss, M., Singer, H., Hollender, J., 2010. LC–high resolution MS in environmental analysis: from target screening to the identification of unknowns. Anal. Bioanal. Chem. 397, 943–951.
Lai, H.-T., Wang, T.-S., Chou, C.-C., 2011. Implication of light sources and microbial activities on degradation of sulfonamides in water and sediment from a marine shrimp pond. Bioresour. Technol. 102, 5017–5023.
Li, X., Zheng, W., Machesky, M.L., Yates, S.R., Katterhenry, M., 2011. Degradation kinetics and mechanism of antibiotic ceftiofur in recycled water derived from a beef farm. J. Agric. Food Chem. 59, 10176–10181.
Li, X., Brownawell, B., 2009. Analysis of quaternary ammonium compounds in estuarine sediments by Lc-ToF-MS: very high positive mass defects of alkylamine ions as powerful diagnostic tools for identification and structural elucidation. Anal. Chem. 81, 7926–7935.
Li, X., Zheng, W., Kelly, W.R., 2013. Occurrence and removal of pharmaceutical and hormone contaminants in rural wastewater treatment lagoons. Sci. Total Environ. 445, 22–28.
Li, X., Wu, K., Gu, S., Jiang, P., Li, H., Liu, Z., Dai, M., 2021. Enhanced biodegradation of dissolved organic carbon in the western boundary Kuroshio Current when intruded to the marginal South China Sea. J. Geophys. Res.: Oceans 126, e2021JC017585.
Little, J.L., Cleven, C.D., Brown, S.D., 2011. Identification of "known unknowns" utilizing accurate mass data and chemical abstracts service databases. J. Am. Soc. Mass Spectrom. 22, 348–359.
Manna, J.D., Richardson, S.J., Moghaddam, M.F., 2017. Implementation of a novel ultra fast metabolic stability analysis method using exact mass TOF-MS. Bioanalysis 9, 359–368.
Maquille, A., Salembier, S., Hérent, M.-F., Jiwan, J.-L.H., 2010. Photodegradation of flupentixol in aqueous solution under irradiation at 254 nm: identification of the photoproducts generated. J. Photochem. Photobiol. Chem. 214, 224–229.
Marie, D., Partensky, F., Jacquet, S., Vaulot, D., 1997. Enumeration and cell cycle analysis of natural populations of marine picoplankton by flow cytometry using the nucleic acid stain SYBR Green I. Appl. Environ. Microbiol. 63, 186–193.
Mi, N., Cheng, T., Li, H., Yang, P., Mu, X., Wang, X., Zu, X., Qi, X., Guo, X., Ye, J., 2019. Metabolite profiling of traditional Chinese medicine formula Dan Zhi Tablet: an integrated strategy based on UPLC-QTOF/MS combined with multivariate statistical analysis. J. Pharmaceut. Biomed. Anal. 164, 70–85.
Morrison Thornton, R., 1983. Organic chemistry. In: Organic Chemistry.4th Ed, fourth ed.
Mortishire-Smith, R.J., O'Connor, D., Castro-Perez, J.M., Kirby, J., 2005. Accelerated throughput metabolic route screening in early drug discovery using high-resolution liquid chromatography/quadrupole time-of-flight mass spectrometry and automated data analysis. Rapid Commun. Mass Spectrom.: An International Journal Devoted to the Rapid Dissemination of Up-to-the-Minute Research in Mass Spectrometry 19, 2659–2670.
Ni, S., Qian, D., Duan, J.-a., Guo, J., Shang, E.-x., Shu, Y., Xue, C., 2010. UPLC–QTOF/MS-based screening and identification of the constituents and their metabolites in rat plasma and urine after oral administration of Glechoma longituba extract. J. Chromatogr. B 878, 2741–2750.
Quintana, J.B., Weiss, S., Reemtsma, T., 2005. Pathways and metabolites of microbial degradation of selected acidic pharmaceutical and their occurrence in municipal wastewater treated by a membrane bioreactor. Water Res. 39, 2654–2664.
Sánchez-Hernández, L., Hernández-Domínguez, D., Martín, M.T., Nozal, M.J., Higes, M., Yagüe, J.L.B., 2016. Residues of neonicotinoids and their metabolites in honey and pollen from sunflower and maize seed dressing crops. J. Chromatogr. A 1428, 220–227.
Sarmah, A.K., Meyer, M.T., Boxall, A.B., 2006. A global perspective on the use, sales, exposure pathways, occurrence, fate and effects of veterinary antibiotics (VAs) in the environment. Chemosphere 65, 725–759.
Sassman, S.A., Lee, L.S., 2005. Sorption of three tetracyclines by several soils: assessing the role of pH and cation exchange. Environ. Sci. Technol. 39, 7452–7459.
Shad, A., Chen, J., Qu, R., Dar, A.A., Bin-Jumah, M., Allam, A.A., Wang, Z., 2020. Degradation of sulfadimethoxine in phosphate buffer solution by UV alone, UV/PMS and UV/H2O2: kinetics, degradation products, and reaction pathways. Chem. Eng. J. 398, 125357.
Shad, A., Li, C., Zuo, J., Liu, J., Dar, A.A., Wang, Z., 2018. Understanding the ozonated degradation of sulfadimethoxine, exploration of reaction site, and classification of degradation products. Chemosphere 212, 228–236.
Singh, S.N., 2012. Microbial Degradation of Xenobiotics. Springer Berlin, Heidelberg.
Tamtam, F., Mercier, F., Le Bot, B., Eurin, J., Dinh, Q.T., Clément, M., Chevreuil, M., 2008. Occurrence and fate of antibiotics in the Seine River in various hydrological conditions. Sci. Total Environ. 393, 84–95.
Tang, G., Liu, M., Zhou, Q., He, H., Chen, K., Zhang, H., Hu, J., Huang, Q., Luo, Y., Ke, H., 2018. Microplastics and polycyclic aromatic hydrocarbons (PAHs) in Xiamen coastal areas: implications for anthropogenic impacts. Sci. Total Environ. 634, 811–820.
Thurman, E.M., Ferrer, I., Zavitsanos, P., Zweigenbaum, J.A., 2013. Identification of imidacloprid metabolites in onion (Allium cepa L.) using high-resolution mass spectrometry and accurate mass tools. Rapid Commun. Mass Spectrom. 27, 1891–1903.
Thurman, E.M., Ferrer, I., Zweigenbaum, J.A., García-Reyes, J.F., Woodman, M., Fernández-Alba, A.R., 2005. Discovering metabolites of post-harvest fungicides in citrus with liquid chromatography/time-of-flight mass spectrometry and ion trap tandem mass spectrometry. J. Chromatogr. A 1082, 71–80.
Trovó, A.G., Nogueira, R.F., Agüera, A., Sirtori, C., Fernández-Alba, A.R., 2009. Photodegradation of sulfamethoxazole in various aqueous media: persistence, toxicity and photoproducts assessment. Chemosphere 77, 1292–1298.
Vaulot, D., Courties, C., Partensky, F., 1989. A simple method to preserve oceanic phytoplankton for flow cytometric analyses. Cytometry: The Journal of the International Society for Analytical Cytology 10, 629–635.
Wang, Y., Liang, J.B., Liao, X.D., Wang, L.-s., Loh, T.C., Dai, J., Ho, Y.W., 2010. Photodegradation of sulfadiazine by goethite-oxalate suspension under UV light irradiation. Ind. Eng. Chem. Res. 49, 3527–3532.
Wang, Q., Guo, M., Yates, S.R., 2006. Degradation kinetics of manure-derived sulfadimethoxine in amended soil. J. Agric. Food Chem. 54, 157–163.
Wei, R., Ge, F., Zhang, L., Hou, X., Cao, Y., Gong, L., Chen, M., Wang, R., Bao, E., 2016. Occurrence of 13 veterinary drugs in animal manure-amended soils in Eastern China. Chemosphere 144, 2377–2383.
Witte, W., 1998. Medical consequences of antibiotic use in agriculture. Science 279, 996–997.
Xiao, S., Wan, J., Wang, Y., Yan, Z., Ma, Y., Sun, J., Tang, M., Cao, J., Chen, J., 2023. Distribution, sources, and risk assessment of emerging contaminants in the effluents from large-scale wastewater treatment plants in guangzhou central districts, south China. Water, air. & Soil Pollution 234, 455.
Xin, X., Sun, S., Zhou, A., Wang, M., Song, Y., Zhao, Q., Jia, R., 2020. Sulfadimethoxine photodegradation in UV-C/H2O2 system: reaction kinetics, degradation pathways, and toxicity. J. Water Proc. Eng. 36, 101293.
Xu, B., Mao, D., Luo, Y., Xu, L., 2011. Sulfamethoxazole biodegradation and biotransformation in the water–sediment system of a natural river. Bioresour. Technol. 102, 7069–7076.
Xu, W.-h., Zhang, G., Zou, S.-c., Li, X.-d., Liu, Y.-c., 2007. Determination of selected antibiotics in the Victoria Harbour and the Pearl River, South China using high-performance liquid chromatography-electrospray ionization tandem mass spectrometry. Environ. Pollut. 145, 672–679.
Zessel, K., Mohring, S., Hamscher, G., Kietzmann, M., Stahl, J., 2014. Biocompatibility and antibacterial activity of photolytic products of sulfonamides. Chemosphere 100, 167–174.
Zhang, Y., Zhao, Z., Dai, M., Jiao, N., Herndl, G.J., 2014. Drivers shaping the diversity and biogeography of total and active bacterial communities in the South China Sea. Mol. Ecol. 23, 2260–2274.
Zheng, S., Qiu, X., Chen, B., Yu, X., Liu, Z., Zhong, G., Li, H., Chen, M., Sun, G., Huang, H., 2011. Antibiotics pollution in Jiulong River estuary: source, distribution and bacterial resistance. Chemosphere 84, 1677–1685.
Zhuang, J., Wang, S., Tan, Y., Xiao, R., Chen, J., Wang, X., Jiang, L., Wang, Z., 2019. Degradation of sulfadimethoxine by permanganate in aquatic environment: influence factors, intermediate products and theoretical study. Sci. Total Environ. 671, 705–713.